IEEE Access
Multidisciplinary ⋮ Rapid Review ⋮ Open Access Journal

Date of publication xxxx 00, 0000, date of current version xxxx 00, 0000.

Digital Object Identifier xx.xxxx/ACCESS.202x.xxxxxxx

Mathematical model for WAVE, an energy harvesting marine surface vehicle

D. DI VITO[1,2], G. GILLINI[2], A. COLLEVECCHIO[3], L. BAZZARELLO[3], A. TRAVERSO[4], A. CAFFAZ[5], G. ANTONELLI[1], (Fellow, IEEE)

[1]ISME, University of Cassino and Southern Lazio, Via Di Biasio 43, 03043 Cassino, Italy (e-mail: d.divito@unicas.it)
[2]EveryBotics Srl, Via Cimarosa 57, 03043 Cassino, Italy
[3]Marina Militare Italiana, Viale San Bartolomeo 400, 19126 La Spezia, Italy
[4]ISME, University of Genova, Via Alla Opera Pia 15, 16145 Genova, Italy
[5]Graal Tech Srl, Via Tagliolini 26, 16152 Genova, Italy

Corresponding author: Daniele Di Vito (e-mail: d.divito@unicas.it)

ABSTRACT WAVE is a multi-propulsion vehicle developed by the Italian Navy which can work as an AUV (Autonomous Underwater Vehicle), a glider and, when at surface, as a wave glider. In this latter configuration, it behaves as a wave-powered autonomous surface vehicle that converts wave-induced motion into forward thrust through appropriately designed submerged wings, either loosely or rigidly connected to the floating body. When additionally equipped with solar panels, wave gliders can be designed for long-endurance missions. This paper presents a six degrees of freedom (DoFs) mathematical model of such a vehicle, featuring two independent wings rigidly connected to the rigid body. The numerical simulations provide theoretical basis and reference for future improvements and parameters identification.

INDEX TERMS Oceanic engineering; marine surface vehicle; wave glider; energy harvesting; modeling and simulation.

I. INTRODUCTION

Wave gliders are autonomous surface platforms characterized by the capability to harvest energy from the oceanic waves. With a proper engineering design a wave glider may exhibit low maintenance features which, together with the long endurance one and proper sensor suite, make this kind of vehicles a promising device for long duration missions. Examples are oceanographic and climate observation, marine mammal monitoring but also harbor security and surveillance for illegal fishing. Among the first prototypes [1], a review can be found, e.g., in [2], [3].

[4] describes modeling and control for a glider characterized by the presence of moving mass in charge of changing to pitch in order to excite the vehicle lift and impose the advancing direction. Determination of hydrodynamic coefficients for an AUV steered by control surfaces is presented in [5]. Lift and drag coefficients for different angles of attack are computed with both computational fluid dynamics software and experiment in a towing tank. [6] uses a probabilistic regression model instead of classical mechanics to capture the vehicle macroscopic behavior. [7] analyzes in detail the wing's forces and discusses optimal design of the wing profile and mechanical limit. [8] presents the model of a wave glider achieved by the Newton-Euler approach. Interesting modeling considerations, similar to the case at hand, have been done. The presence of the tether is also taken into account. The lift coefficient is modelled with a linear+quadratic term in the angle of attack. The dynamic characteristics of the transit stage between the falling and rising phases of the hydrofoils are not considered. [9], [10] devotes a PhD thesis for the modeling and identification of the mathematical model of a wave glider. The wave generated thrust is modeled as a random force shaped according to a Gaussian probability distribution function.

The wing optimal configuration in terms of maximum range is analyzed in, e.g. [7] where a 6 DoFs mathematical model is also presented for a wave glider composed by two hulls loosely connected. The submerged hull carries a set of connected wings.

This paper presents the 6 DoFs mathematical model for WAVE, a vehicle developed by the Italian Navy as improvement of the one previously developed and discussed in [11]–[13]. WAVE is a multi-propulsion vehicle, it can act as an AUV (Autonomous Underwater Vehicle), ad a glider and, when at surface, as a wave glider. The latter configuration is of interest in this paper. In the reference above, beyond the different wings position and shape, the mathematical model considers the vehicle dynamics restricted to the vertical

This article has been accepted for publication in IEEE Access. This is the author's version which has not been fully edited and
content may change prior to final publication. Citation information: DOI 10.1109/ACCESS.2026.3702412

plane derived via a non-standard Lagrangian approach. In the following, instead, the inverse dynamics model is obtained by resorting to a Newton-Euler approach that is eventually verified through numerical simulations.

This work is organized as follows. Section II shows both the kinematic and dynamic model of the WAVE system and presents the ocean wave modeling focusing on the interaction of the latter with the vehicle, i.e., forces acting on wings (lift and drag) and system buoyancy. Section III reports the vehicle characteristics in terms of dynamic parameters. Finally section IV shows the results obtained through the numerical simulations performed in different operative conditions.

It is worth noticing that, since the proposed model is mainly defined through literature well known physical concepts and it does not result from an identification process of WAVE system dynamic parameters as well as of the lift and drag coefficients, which determine the forces acting on vehicle wings, the obtained numerical results should be considered qualitatively and not quantitatively.

II. MODELING

In the following both the kinematic and dynamic modeling are presented for the WAVE robot vehicle and the ocean wave.

A. REFERENCE FRAMES

Fig. 1 reports the inertial frame Σ_I, defined according to the North-East-Down (NED) convention [14], the body-fixed frame Σ_B and the wings-fixed frames together with their respective positive verse of rotation. In particular, Σ_B is fixed in the geometrical center of the WAVE vehicle, while the wings frames are set on their axis of rotation to comply with the Denavit-Hartenberg convention [15] and facilitate the dynamic modeling part.

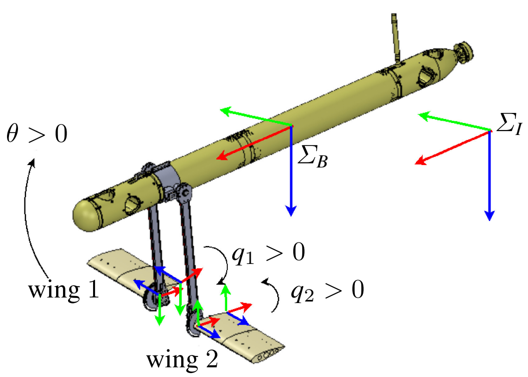

FIGURE 1. Vehicle and its body-fixed principal frames.

B. KINEMATICS

Positioning of a rigid-body with respect to a reference frame $\Sigma_I, O-xyz$ that it is supposed to be earth-fixed and inertial is achieved by using 3 coordinates grouped in a vector, i.e., by defining $\boldsymbol{\eta}_1 \in \mathbb{R}^3$:

$$\boldsymbol{\eta}_1 = \begin{bmatrix} x \\ y \\ z \end{bmatrix}.$$

Let define $\boldsymbol{\eta}_2 \in \mathbb{R}^3$ as

$$\boldsymbol{\eta}_2 = \begin{bmatrix} \phi \\ \theta \\ \psi \end{bmatrix}$$

the vector of body Euler-angle coordinates in an earth-fixed reference frame. In the (aero)nautical field those are commonly named roll, pitch and yaw angles and corresponds to the elementary rotation around x, y and z in fixed frame [14].

The two wings are considered as two one-link manipulator and labeled according to the Denavit-Hartenberg convention. Their joint positions, denoted with q_1 and q_2, follows accordingly. Fig. 1 reports the zero for both joints together with their positive sense of rotation. The system configuration is denoted as

$$\boldsymbol{q} = \begin{bmatrix} \boldsymbol{\eta}_1^{\mathrm{T}} & \boldsymbol{\eta}_2^{\mathrm{T}} & q_1 & q_2 \end{bmatrix}^{\mathrm{T}} \in \mathbb{R}^8. \tag{1}$$

The velocity is defined as

$$\boldsymbol{\zeta} = \begin{bmatrix} \dot{\boldsymbol{\eta}}_1^{\mathrm{T}} & \boldsymbol{\omega}^{\mathrm{T}} & \dot{q}_1 & \dot{q}_2 \end{bmatrix}^{\mathrm{T}} \in \mathbb{R}^8 \tag{2}$$

where $\boldsymbol{\omega} \in \mathbb{R}^3$ denotes the vehicle angular velocity expressed in the inertial frame, and not the time derivative of the vehicle orientation expressed in Roll-Pitch-Yaw (RPY) angles.

C. OCEAN WAVE

According to [16] the wave's height is defined as

$$h = h(x, y, t) = -A\cos(kx - \omega_w t) \quad \text{m} \tag{3}$$

where $A > 0$ is the wave amplitude, k is the wave number expressed in rad/m and ω_w the frequency expressed in rad/s. When $k > 0$ the wave moves to positive x. The wavelength is defined as $\lambda = \frac{2\pi}{|k|}$ and the wave period as $T = \frac{2\pi}{\omega_w}$. The assumption

$$A\,|k| << 1$$

will be made, i.e., the wave is *linear* and exhibits a small slope.

By assuming also *deep water waves*, i.e., wave amplitude much smaller than the water depth, the wave frequency is related to the wave number by

$$k = \frac{\omega_w^2}{\|\boldsymbol{g}\|} \tag{4}$$

where $\boldsymbol{g} \in \mathbb{R}^3$ is the gravity.

The wave's velocity is described by the following

$$\boldsymbol{\nu}_c = A\omega_w e^{-kz} \begin{bmatrix} \cos(kx - \omega_w t) \\ 0 \\ -\sin(kx - \omega_w t) \end{bmatrix} \quad \text{m/s} \tag{5}$$

where it can be noted that the wave exhibits null y component and it vanishes with the depth.

This article has been accepted for publication in IEEE Access. This is the author's version which has not been fully edited and content may change prior to final publication. Citation information: DOI 10.1109/ACCESS.2026.3702412

D. DYNAMICS

Equations of motion of the system can be written in matrix form as [17]:

$$\boldsymbol{M}(\boldsymbol{q})\dot{\zeta} + \boldsymbol{C}(\boldsymbol{q}, \zeta_r)\zeta_r + \boldsymbol{D}(\boldsymbol{q}, \zeta_r)\zeta_r + \boldsymbol{g}(\boldsymbol{q}, \boldsymbol{R}_B^I) = \boldsymbol{\tau} \tag{6}$$

where $\boldsymbol{M} \in \mathbb{R}^{8\times 8}$ is the inertia matrix including added mass terms, $\boldsymbol{C}(\boldsymbol{q}, \boldsymbol{\zeta})\boldsymbol{\zeta} \in \mathbb{R}^8$ is the vector of Coriolis and centripetal terms, $\boldsymbol{D}(\boldsymbol{q}, \boldsymbol{\zeta})\boldsymbol{\zeta} \in \mathbb{R}^8$ is the vector of dissipating effects, $\boldsymbol{g}(\boldsymbol{q}, \boldsymbol{R}_B^I) \in \mathbb{R}^8$ is the vector of gravity and buoyancy effects. In (6) the relative velocity $\boldsymbol{\zeta}_r$ is used to take into account the interaction with the water. The right hand side of the equation is null in our case due to the absence of thrusters, i.e., $\boldsymbol{\tau} = \boldsymbol{0}$. It is worth noticing that several wave-gliders are designed with a small propeller to provide a *small* linear force along x_v [18].

Equation (6), i.e., the model inverse dynamics, can be obtained in symbolic form via, e.g., a Lagrangian formulation as done in [11]. However, in order to be more flexible with the choice of the parameters and to adapt easily with respect to eventual changes in the wings design it has been preferred to implement the inverse dynamic by resorting to a Newton-Euler approach [17], [19]. Shortly, the overall system wrenches are obtained by properly propagating numerically velocities, accelerations and forces at each sampling time without computing in symbolic the matrices involved in (6) as detailed in Section IV.

E. WING FORCES

In addition to the inertial forces, the added mass and the gravity-buoyancy contribution, the wings are subject to the drag and lift forces.

Drag can be modeled according to [14] as:

$$\boldsymbol{f}_D = \frac{1}{2}\rho C_D S \|\boldsymbol{v}\| \boldsymbol{v} \tag{7}$$

where ρ is the density of the water, S is the projected wing's area on the flow direction, $\boldsymbol{v} \in \mathbb{R}^3$ is the flow velocity and C_D is the drag coefficient. It is worth noticing that the latter is a function of several variables, such as the Reynold's number, the wing's shape and the angle of attack, i.e., the angle between the flow direction and the wing's chord being coincident with its axis of symmetry for the case at hand (see Fig. 2).

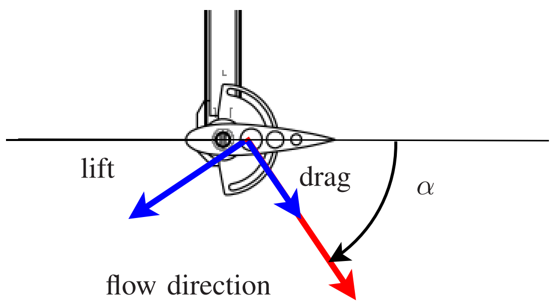

FIGURE 2. Planar rendering of the lift and drag forces (in blue) and the relative velocity (in red) which are further inserted in the Newton-Euler computation of the inverse dynamics.

Typical values of C_D range from nearly zero to about $1-2$. In particular, Fig. 3 reports an approximation of the experimental identification computed in [20] for the symmetric NACA airfoil section 0015 at different Reynold's number around 10^5.

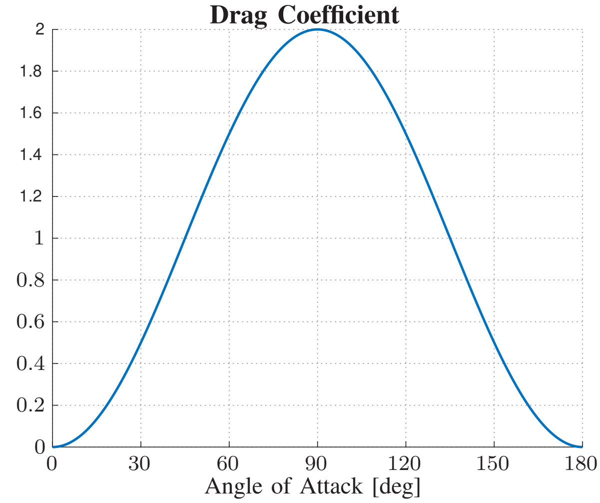

FIGURE 3. Drag coefficient as function of the angle of attack as reported in [20].

Similarly, also a lift force needs to be considered as [21]

$$\boldsymbol{f}_L = \frac{1}{2}\rho C_L S \|\boldsymbol{v}\| \boldsymbol{v}^{\perp} \tag{8}$$

where the direction should be chosen normal to the flow in the direction of the low-pressure side as shown in Fig. 2.

The lift and drag coefficient are function, among the others, of the angle of attack and the wing's shape, a NACA 0021 in this case [22]. The L/D ratio, i.e., the ratio of the module between those two forces is of order of magnitude 10 for light air crafts. It is worth noticing that the sinusoidal shape of the wave and the wing's movement excite angles much larger than the interval usually computed for the aeronautical field.

Fig. 4 reports the approximation of an experimental identification computed in [20] for the symmetric NACA airfoil section 0012H at Reynold's number around 10^5.

Another possibility is to model the lift coefficient as a constant term plus a term linear in the angle of attack as in [4].

It is worth noticing that, due the complexity of the phenomenon, a probabilistic force generation is also proposed to model wave gliders propulsion [10] which is mainly given by the lift.

F. BUOYANCY

When a rigid body is submerged in a fluid under the effect of the gravity two more forces have to be considered: the gravitational force and the buoyancy. The latter is the only hydrostatic effect, i.e., it is not function of a relative movement between body and fluid.

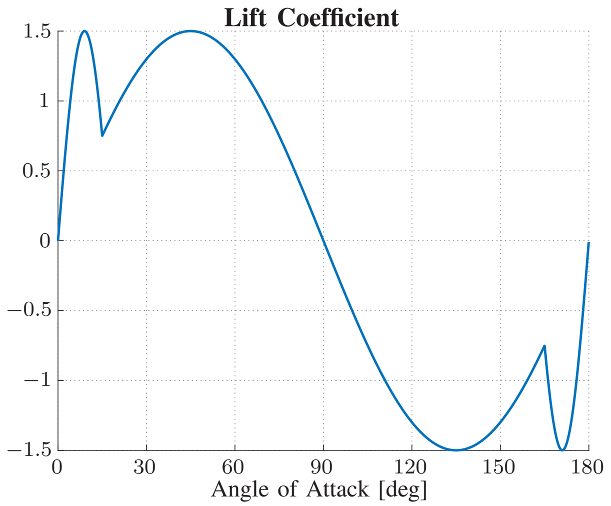

FIGURE 4. Lift coefficient as function of the angle of attack as reported in [20].

Let us define as

$$\boldsymbol{g}^I = \begin{bmatrix} 0 \\ 0 \\ 9.81 \end{bmatrix} \text{m/s}^2$$

the acceleration of gravity, ∇ the volume of the body and m its mass. The submerged weight of the body is defined as $W = m\left\|\boldsymbol{g}^I\right\|$ while its buoyancy $B = \rho\nabla\left\|\boldsymbol{g}^I\right\|$.

The gravity force, acting in the center of mass $\boldsymbol{r}_C^B$ is represented in body-fixed frame by:

$$\boldsymbol{f}_G(\boldsymbol{R}_B^I) = \boldsymbol{R}_I^B \begin{bmatrix} 0 \\ 0 \\ W \end{bmatrix},$$

while the buoyancy force, acting in the center of buoyancy $\boldsymbol{r}_B^B$ is represented in body-fixed frame by:

$$\boldsymbol{f}_B(\boldsymbol{R}_B^I) = -\boldsymbol{R}_I^B \begin{bmatrix} 0 \\ 0 \\ B \end{bmatrix}.$$

The (6×1) vector of force/moment due to gravity and buoyancy in body-fixed frame, included in the left hand-side of the equations of motion, is represented by:

$$\boldsymbol{g}_{RB}(\boldsymbol{R}_B^I) = -\begin{bmatrix} \boldsymbol{f}_G(\boldsymbol{R}_B^I) + \boldsymbol{f}_B(\boldsymbol{R}_B^I) \\ \boldsymbol{r}_G^B \times \boldsymbol{f}_G(\boldsymbol{R}_B^I) + \boldsymbol{r}_B^B \times \boldsymbol{f}_B(\boldsymbol{R}_B^I) \end{bmatrix}.$$

In this study, buoyancy is computed assuming a finite-element approach and exploiting the assumptions of wave small slope (see sect. II-C). The vehicle hull is modeled as an ellipsoid and its submerged volume computed by discretizing the hull. The latter computation is done by intersecting the wave assumed locally constant with the hull. Based on the submerged volume knowledge, both the buoyancy and the new center of buoyancy can be computed and used for the inverse dynamics.

The approximation embedded in this computation is based on several factors: the effective volume shape, the small slope wave and the vehicle length. Fig. 5 shows a planar rendering of a typical computation with the wave height $h = -0.1$ m, the vehicle position and orientation $\boldsymbol{\eta} = \begin{bmatrix} 3 & 3 & 0.15 & 0 & 20 & -30 \end{bmatrix}^{\mathrm{T}}$ [m, deg], the dry and the wet center of buoyancy for the current configuration are shown, in this configuration the submerged volume is 88 % of the dry volume.

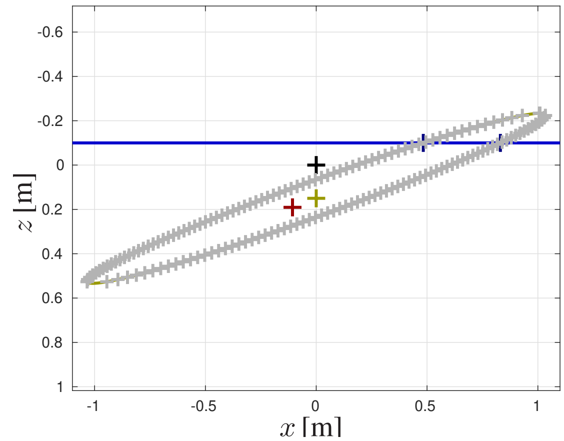

FIGURE 5. Planar rendering of the buoyancy computation for a sample configuration, the dry and the wet center of buoyancy for the such configuration are shown in yellow and red, respectively.

G. HULL DRAG

Damping is computed by considering the ocean current, i.e., the wave velocity, rotated in body-fixed frame such that the relative velocity is used in the computation of the linear and quadratic damping. The wave velocity value at the vehicle position is assumed thus approximating its effect within the vehicle hull. The wrench applied is then proportional to the effective submerged body. The term in (6) is then computed by considering a diagonal damping matrix and the individual effect is

$$\alpha\left(d_{l,i}\zeta_{r,i} + d_{q,i}\left|\zeta_{r,i}\right|\zeta_{r,i}\right) \tag{9}$$

where $d_{l,i}$ and $d_{q,i}$ are the linear and quadratic damping coefficients, respectively, the index i denotes the degree of freedom and $\alpha \in [0, 1]$ the ratio of the submerged body.

III. VEHICLE CHARACTERISTICS

The dry weight of the vehicle under study, without wings, is 30 kg, each wing weights 3 kg. The overall design is such that the positive buoyancy is ≈ 0.3 kg. The center of gravity is located in

$$\boldsymbol{r}_G = \begin{bmatrix} 0 & 0 & 0.05 \end{bmatrix}^{\mathrm{T}} \quad \text{m} \tag{10}$$

The vehicle damping coefficients have been simulated as:

$$\boldsymbol{D}_l = \text{diag}\begin{bmatrix} 2.5 & 15 & 15 & 5 & 10 & 10 \end{bmatrix}$$

for the linear and

$$\boldsymbol{D}_q = \text{diag}\begin{bmatrix} 25 & 325 & 325 & 10 & 40 & 40 \end{bmatrix}$$

for the quadratic damping.

The vehicle is modeled as an ellipsoid characterized by dimensions 1.1 m along body-fixed x and 8 cm along the other directions. The 6×6 mass matrix, including the added mass, follow consequently as reported in [17]:

$$\boldsymbol{M}_{RB} = \begin{bmatrix} 30 & 0 & 0 & 0 & 1.5 & 0 \\ 0 & 30 & 0 & -1.5 & 0 & 0 \\ 0 & 0 & 30 & 0 & 0 & 0 \\ 0 & -1.5 & 0 & 0.08 & 0 & 0 \\ 1.5 & 0 & 0 & 0 & 7.3 & 0 \\ 0 & 0 & 0 & 0 & 0 & 7.3 \end{bmatrix}$$

and

$$\boldsymbol{M}_{A} = \begin{bmatrix} 0.65 & 0 & 0 & 0 & 0 & 0 \\ 0 & 28.76 & 0 & 0 & 0 & 0 \\ 0 & 0 & 28.76 & 0 & 0 & 0 \\ 0 & 0 & 0 & 0 & 0 & 0 \\ 0 & 0 & 0 & 0 & 6.42 & 0 \\ 0 & 0 & 0 & 0 & 0 & 6.42 \end{bmatrix}$$

The wings dimension is $20 \times 45 \times 3$ cm and they are designed to be neutrally buoyant with center of gravity coincident with the center of buoyancy.

The joint's friction coefficient is 0.1 Ns/rad. Drag and lift have been modeled as reported in Fig. 3 and 4. This assumption has been motivated by similar qualitative behaviour of C_D and C_L. In fact, without an experimental identification and being the angle of attack larger than the range usually considered for the aeronautical field, it has not been possible to exactly model these coefficients.

The mechanical joint limit for the wing can be fixed in a range typically smaller than ± 70 deg.

IV. NUMERICAL SIMULATION

The numerical simulation of the WAVE's dynamics has been obtained by adapting SIMURV, the simulator developed in [17]. The main modification consists in adding two interaction points on the vehicle hull, representing the two wings, which are modeled as two 1-link unactuated robots. One advantage of adapting SIMURV is the ability to easily modify any simulator parameter without recompiling or rewriting the equations.

Assuming that the inverse dynamics in (6) can be computed using a recursive Newton-Euler approach, the direct dynamics is obtained as

$$\dot{\boldsymbol{\zeta}} = \boldsymbol{M}(\boldsymbol{q})^{-1}(\boldsymbol{\tau} - \boldsymbol{\tau}_n) \ , \tag{11}$$

without resorting to the symbolic matrix $\boldsymbol{M} \in \mathbb{R}^{8\times 8}$ [23], [24] (see Algorithm 1).

The vehicle at hand has been designed such that the pitch is null in steady state in absence of external disturbances with a light positive buoyancy. The wings and the fixed link supporting them have been designed to be neutrally buoyant. Concerning the buoyancy computation in sect. II-F, for the numerical case under study an error of the order of the centimeter in the computation of the buoyancy can be assumed.

Algorithm 1 Direct Dynamics resorting only to Inverse Dynamics

```
acc ← 0
τ_n ← InverseDynamics
g ← 0
for i = 1 to 8 do
    vel ← 0
    acc ← 0
    acc[i] ← 1
    M(:, i) ← InverseDynamics
end for
g ← 9.81
acc ← M^{-1} · (τ − τ_n)
```

The changes of the wave velocity along the hull are estimated in mm/s and have been assumed to be constant along the hull itself.

Then, a simulative campaign has been performed focusing on the following case studies:

- Nominal case;
- Change-Wing-Joint-Limits case;
- Change-Wing-Area case;
- Change-Wave-Frequency case;
- Change-Wave-Amplitude case.

The glider initial state is equal for each considered scenario, i.e., with position

$$\boldsymbol{\eta}_1 = \begin{bmatrix} 0 & 0 & 0.05 \end{bmatrix}^{\mathrm{T}} \text{ m}$$

and orientation

$$\boldsymbol{\eta}_2 = \begin{bmatrix} 0 & 0 & 180 \end{bmatrix}^{\mathrm{T}} \text{ deg.}$$

A. NOMINAL CASE

It represents a case where a significant forward velocity countercurrent is obtained. The operative conditions are:

- wing joint limit: 20 deg;
- wing area: 0.20×0.45 m;
- wave frequency ω_w: 2.5 rad/s;
- wave number $k = 0.6$ rad/m ($\lambda \approx 10$ m);
- wave amplitude A: 0.25 m.

In such scenario the vehicle forward velocity is $\sim$ 10 cm/s. In fact, as noticeable in Fig. 6a) the system reaches about 3 m in 30s keeping, as expected, its roll $\phi = 0$ deg and yaw $\psi = 180$ deg, while the pitch swings due to the ocean wave. Fig. 6b) shows the wings positions, q_1, q_2, where the oscillatory behaviors between the mechanical joint limits is remarkable. This actually represents the desired condition since in this situation the lift force given by the interaction of the wave with wings is appropriate in the countercurrent direction. Fig. 6c) reports the vehicle linear velocity and the wing angular velocity, respectively, while in Fig 6d) the ocean wave velocity and height are shown. The lift forces applying on wings are finally presented in Fig 6e), 6f) with the corresponding angles of attack.

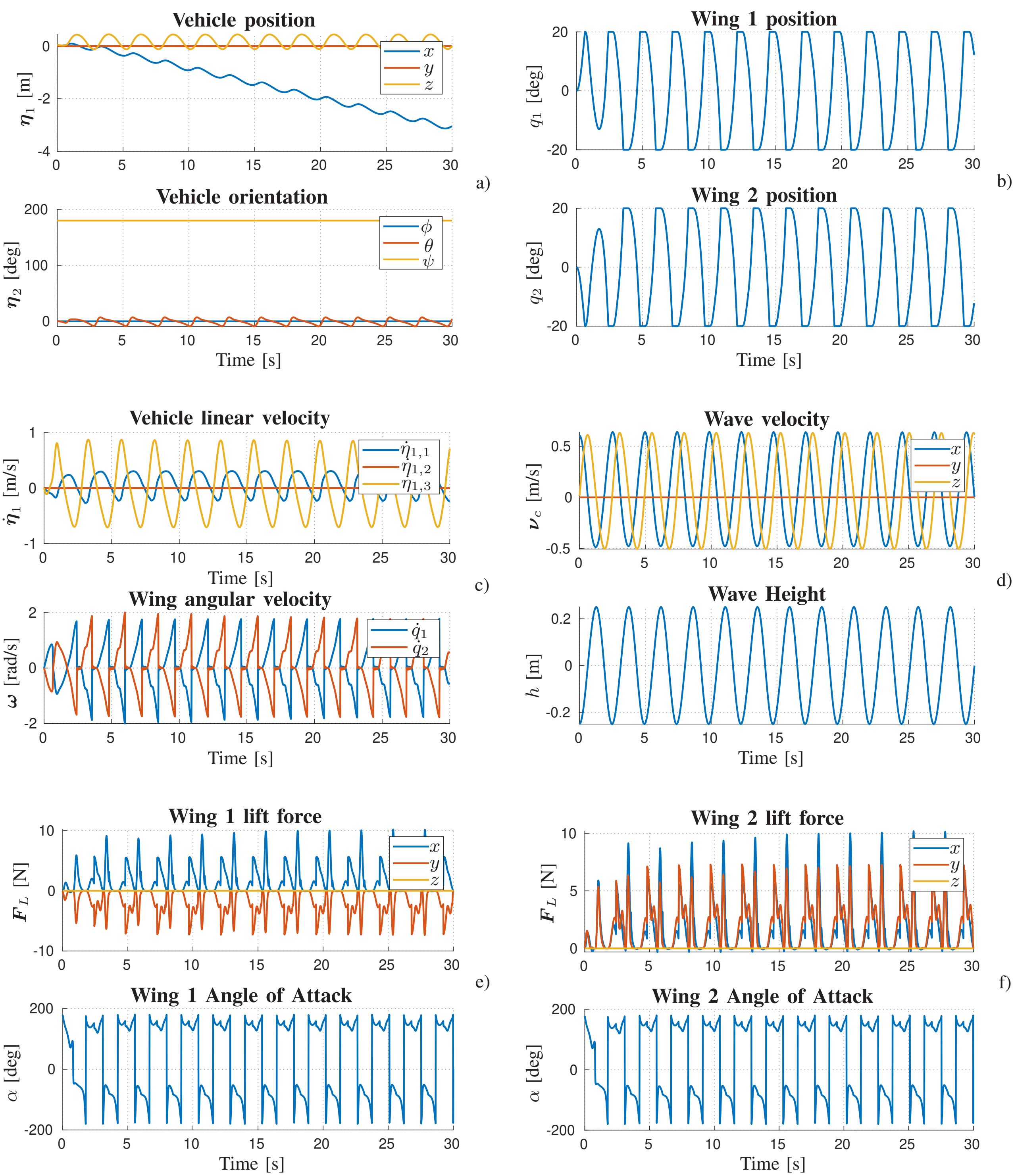

FIGURE 6. **Nominal Case simulation results: a) vehicle position and orientation; b) wings positions, i.e., joints positions; c) vehicle linear velocity and wings angular velocity, i.e., joints velocity; d) wave velocity and height; e) lift force and corresponding angle of attack with respect to wing 1 and 2, respectively, expressed in wing frame.**

B. CHANGE-WING-JOINT-LIMITS CASE

In this scenario, using the same operative conditions of the Nominal case, the joint mechanical limit is changed to observe the different system response. In detail, the following values are used:

- wing joint limit: $\begin{bmatrix}20 & 30 & 45 & 60\end{bmatrix}$ deg;
- wing area: 0.20×0.45 m;
- wave frequency ω_w: 2.5 rad/s;
- wave number $k = 0.6$ rad/m ($\lambda \approx 10$ m);
- wave amplitude A: 0.25 m.

The simulation results are reported in Fig. 7. In particular, from the left figure it is noticeable that the increase of the joint limit beyond 30 deg drastically reduces and even deletes the velocity countercurrent. This behavior is evident in the right figure where the vehicle forward velocity is reported. For $20, 30$ deg the latter is countercurrent (negative value) whereas for $45, 60$ deg it is directed along the ocean current flow (positive value), i.e., the glider is not advancing as desired. Moreover in the same figure the lift norm average is reported, showing qualitatively how the lift performs with different mechanical joints.

It should be noticed that the behavior is due to the coupling of several effects, the wings may not oscillate between the limits due to the joint friction, the wave amplitude and frequency.

Another effect to be taken into account is the vehicle's pitch movement. This is mainly caused by the buoyancy and, when the pitch movement is too high, it may interfere with a proper wing movement contributing to the shown effect. It should be remembered that the buoyancy dynamics is also affected by a certain approximation and matching with the real vehicle with parameters tuning may eventually lead to different quantitative results.

C. CHANGE-WING-AREA CASE

Similarly to the previous case study, the Nominal case values are used except the wing area, increased to analyse the effect on the lift force which is function, among the others, of the wing surface S (see eqs. (7) and (8)). The conditions are listed below:

- wing joint limit: 20 deg;
- wing area: 0.20×0.45 m $\begin{bmatrix}\times 1 & \times 2 & \times 4\end{bmatrix}$;
- wave frequency ω_w: 2.5 rad/s;
- wave number $k = 0.6$ rad/m ($\lambda \approx 10$ m);
- wave amplitude A: 0.25 m.

Fig. 8 reports the numerical results for the x component of $\boldsymbol{\eta}_1$ and the wing 1 position (left plots). In detail, it is noticeable that increasing the wing surface the glider is able to move faster as well, as shown in the right plots in Fig. 8. However, the forward velocity saturates after the increasing factor $\times 3$, even if the lift force is getting larger. This implies that the drag force is increasing as well, compensating for the lift one. It must be remarked that the overall behavior is based on assumptions made on the lift and drag forces, their shape and maximum values influence significantly the simulation output.

Regarding the wing movements, they are quite similar to the nominal case since, due to the assumptions made, their dynamics is not affected by the area.

D. CHANGE-WAVE-FREQUENCY CASE

In this case study, starting from the nominal one, the wave frequency ω_w is changed to inspect the system reaction to different ocean wave conditions. In particular, the following values are used:

- wing joint limit: 20 deg;
- wing area: 0.20×0.45 m;
- wave frequency ω_w: $\begin{bmatrix}1.5 & 2.0 & 2.5 & 3.0\end{bmatrix}$ rad/s;
- wave number $k = 0.6$ rad/m ($\lambda \approx 10$ m);
- wave amplitude A: 0.25 m.

Fig. 9 shows the numerical results for the current case study. It is clear from the plots that both low and high frequency are not optimal for the generation of lift force and, thus, for the glider passive propulsion. In fact, on the one hand, the lowest tested frequency, i.e., $\omega_w = 1.5$ rad/s, results in a wave period of $T = 4.19$ s with a consequent oscillation too slow for properly exciting the interaction with glider wings. On the other hand, the highest tested frequency, i.e., $\omega_w = 3.0$ rad/s, results in a wave period of $T = 2.09$ s which, given the wave height, could be reasonably too fast to allow a full interaction between wings and the same wave.

E. CHANGE-WAVE-AMPLITUDE CASE

For the last case study, as done previously, the ocean wave amplitude is changed keeping other parameters constant and equal to the nominal case:

- wing joint limit: 20 deg;
- wing area: 0.20×0.45 m;
- wave frequency ω: 2.5 rad/s;
- wave number $k = 0.6$ rad/m ($\lambda \approx 10$ m);
- wave amplitude A: $\begin{bmatrix}0.15 & 0.20 & 0.25 & 0.30\end{bmatrix}$ m.

The simulations results are reported in Fig. 10. Even in this case it is possible to observe a *pattern* similar to the one seen in the previous scenario changing the wave frequency. In fact, a lower amplitude, i.e., $A = 0.15$ m, seems to be not sufficient for generating propulsive lift forces on the two wings as well as a higher amplitude causes combined with the glider buoyancy causes the wing stall around the joint mechanical limit. In the latter condition, even if the lift force looks larger, there are other factors, e.g., damping and drag effects, that reduce the overall passive propulsion.

V. FUTURE WORK

Future work will include a dedicated experimental campaign at the "Centro di Supporto alla Sperimentazione Navale" (CSSN) of the Italian Navy, located in La Spezia, Italy, where the vehicle and the wave generator shown in Fig. 11 are already available. In particular, the right picture in Fig. 11 shows the WAVE robot with the two wings subsystem; the

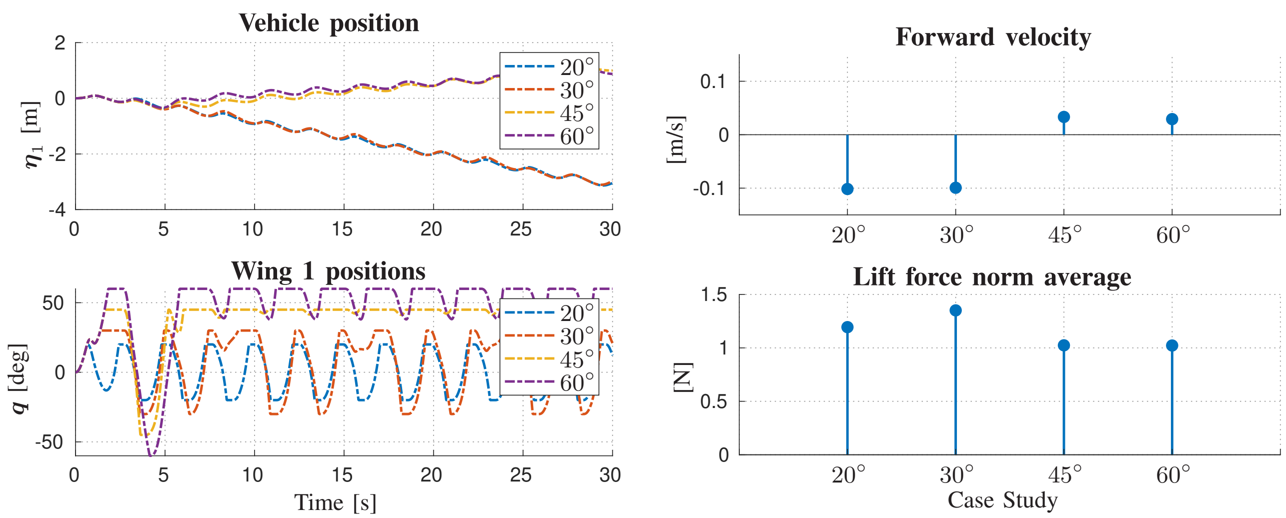

FIGURE 7. **Change-Wing-Joint-Limits Case simulation results obtained by changing the mechanical joint limit in the set [20°, 30°, 45°, 60°]: the vehicle position x components and wing 1 joint positions on the left; vehicle forward velocities (countercurrent) and lift force norm average on the right.**

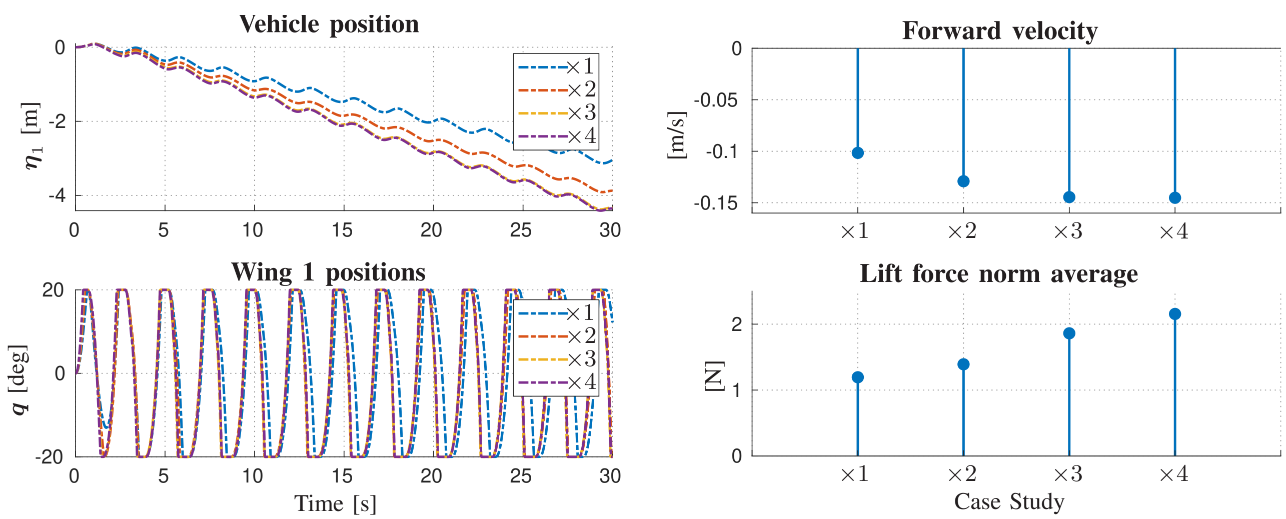

FIGURE 8. **Change-Wing-Area Case simulation results obtained by changing the wing area by increasing the nominal area 0.2×0.45 m by a factor $\times 1$, $\times 2$, $\times 4$, respectively: vehicle position x components and wing 1 joint positions on the left; vehicle forward velocities (countercurrent) and lift force norm average on the right.**

left one illustrates the wave generator together with the origin of a suitably defined reference frame located on the dock, with the x-axis oriented normal to the shoreline. Despite the availability of the experimental infrastructure, the current setup does not allow to collect all the data required for model validation. Therefore, a specifically designed and properly instrumented experimental campaign will be the subject of future work, with the objective of enabling quantitative assessment of the proposed dynamic model and identification of its key parameters, especially those related to the lift force. The experimental results will also provide a basis for refining the model and improving its predictive capability.

VI. CONCLUSIONS

This paper presented a 6 DoFs mathematical model of the WAVE vehicle in wave glider configuration, developed within a Newton–Euler framework to describe the coupled effects of rigid-body dynamics, buoyancy variation, and lift/drag forces generated by the two rigidly connected wings. The proposed model provides a useful representation of passive wave-energy harvesting propulsion for this class of marine surface vehicles.

The numerical results showed that vehicle behavior is strongly influenced by both design and environmental parameters, including wing joint limits, wing area, wave frequency, and wave amplitude. In particular, the analysis highlighted the existence of operating conditions that favor effective propulsion and others that degrade performance because of insufficient excitation, increased drag, or unfavorable vehicle–wing coupling.

Although the present formulation is mainly intended for qualitative analysis, due to the lack of experimental identifi-

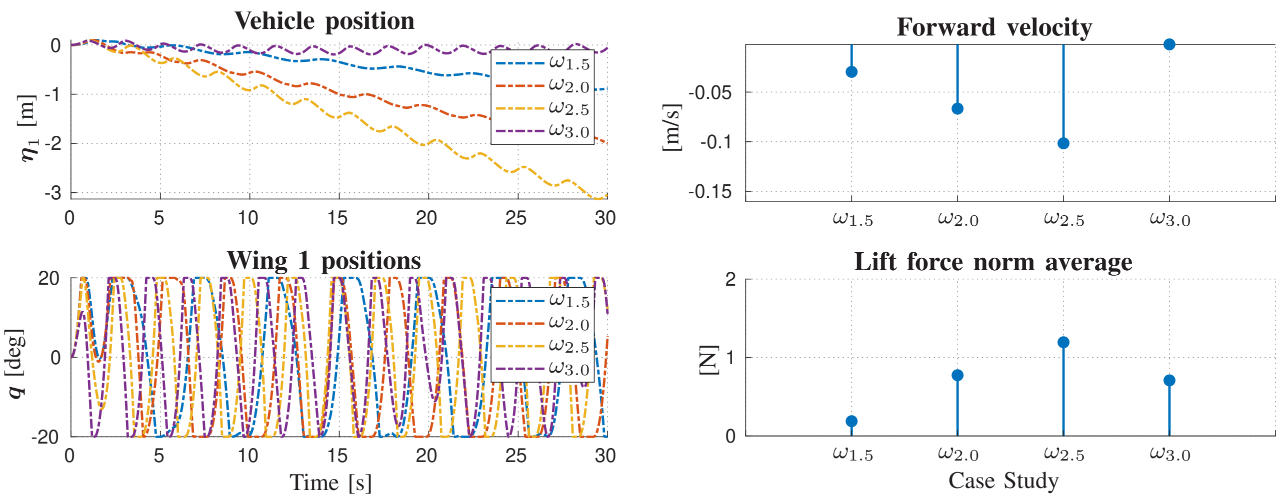

FIGURE 9. **Change-Wave-Frequency Case simulation results obtained by changing the wave frequency in the set $[1.5, 2.0, 2.5, 3.0]$ rad/s: vehicle position x components and wing 1 joint positions on the left; vehicle forward velocities (countercurrent) and lift force norm average on the right.**

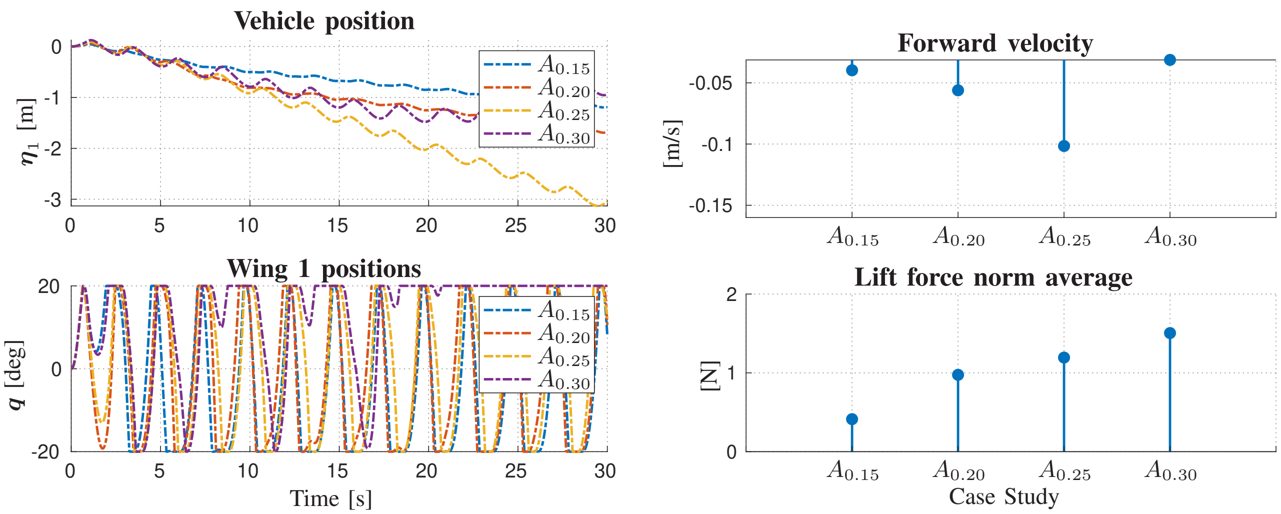

FIGURE 10. **Change-Wave-Amplitude Case simulation results obtained changing the wave amplitude in the set $[0.15, 0.20, 0.25, 0.30]$ m: vehicle position x components and wing 1 joint positions; vehicle forward velocities (countercurrent) and lift force norm average.**

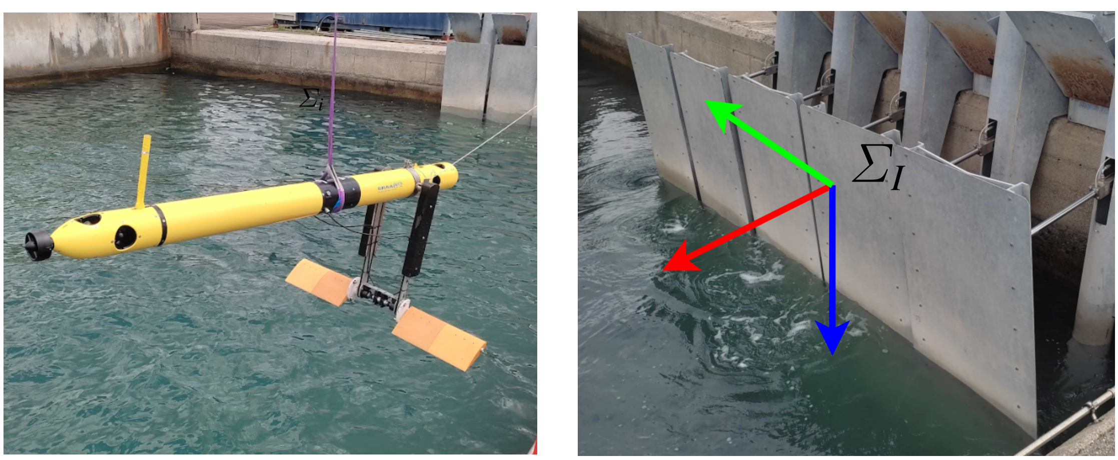

FIGURE 11. **The WAVE glider (on the left) and the ocean wave generator (on the right) with the inertial frame Σ_I used for the experiments at the CSSN of the Italian Navy, located in La Spezia, Italy.**

cation of key hydrodynamic parameters and lift/drag coefficients, it already offers a valuable tool for design support and simulator-based investigation. Future experimental validation will allow parameter identification, quantitative assessment, and further refinement of the model predictive capabilities.

REFERENCES

[1] K. Kawaguchi, Y. Tomoda, H. Kobayashi, and T. Ura, "Development and sea trials of a shuttle type AUV ALBAC," in *International Symposium on Unmanned Untethered Submersible Technology*. Citeseer, 1993, pp. 7–7.

[2] M. Y. Javaid, M. Ovinis, T. Nagarajan, and F. B. Hashim, "Underwater gliders: a review," in *MATEC Web of Conferences*, vol. 13. EDP Sciences, 2014, p. 02020.

[3] D. Meyer, "Glider technology for ocean observations: A review," *Ocean Science Discussions*, vol. 2016, pp. 1–26, 2016.

[4] J. G. Graver and N. E. Leonard, "Underwater glider dynamics and control," in *12th international symposium on unmanned untethered submersible technology*, 2001, pp. 1–14.

[5] E. Javanmard, S. Mansoorzadeh, A. Pishevar, and J. Mehr, "Determination of drag and lift related coefficients of an auv using computational and experimental fluid dynamics methods," *International Journal of Maritime Engineering*, vol. 162, no. A2, 2020.

[6] P. Ngo, J. Das, J. Ogle, J. Thomas, W. Anderson, and R. N. Smith, "Predicting the speed of a wave glider autonomous surface vehicle from wave model data," in *2014 IEEE/RSJ International Conference on Intelligent Robots and Systems*. IEEE, 2014, pp. 2250–2256.

[7] J. Chen, Y. Ge, C. Yao, and B. Zheng, "Dynamics modeling of a wave glider with optimal wing structure," *IEEE Access*, vol. 6, pp. 71 555–71 565, 2018.

[8] P. Wang, X. Tian, W. Lu, Z. Hu, and Y. Luo, "Dynamic modeling and simulations of the wave glider," *Applied Mathematical Modelling*, vol. 66, pp. 77–96, 2019.

[9] N. Kraus and B. Bingham, "Estimation of wave glider dynamics for precise positioning," in *OCEANS'11 MTS/IEEE KONA*. IEEE, 2011, pp. 1–9.

[10] N. D. Kraus, "Wave glider dynamic modeling, parameter identification and simulation," Ph.D. dissertation, [Honolulu]:[University of Hawaii at Manoa],[May 2012], 2012.

[11] A. Caiti, V. Calabrò, S. Grammatico, A. Munafò, and M. Stifani, "Lagrangian modeling of the underwater wave glider," in *OCEANS 2011 IEEE-Spain*. IEEE, 2011, pp. 1–6.

[12] D. Fenucci, A. Caffaz, R. Costanzi, E. Fontanesi, V. Manzari, L. Sani, M. Stifani, D. Tricarico, A. Turetta, and A. Caiti, "WAVE: A wave energy recovery module for long endurance gliders and auvs," in *OCEANS 2016 MTS/IEEE Monterey*. IEEE, 2016, pp. 1–5.

[13] A. Caiti, R. Costanzi, D. Fenucci, V. Manzari, A. Caffaz, and M. Stifani, "WAVE module for hybrid oceanographic autonomous underwater vehicle–prototype experimental validation and characterisation," in *Conference Proceedings of iSCSS*, 2018.

[14] T. Fossen, *Marine Control Systems: Guidance, Navigation and Control of Ships, Rigs and Underwater Vehicles*. Trondheim, Norway: Marine Cybernetics, 2002.

[15] L. Sciavicco and B. Siciliano, *Modelling and control of robot manipulators*. Springer Science & Business Media, 2012.

[16] R. Salmon, "Introduction to ocean waves," *Scripps Institution of Oceanography, University of California, San Diego*, 2008.

[17] G. Antonelli, *Underwater robots*, 4th ed. Heidelberg, D: Springer Tracts in Advanced Robotics, Springer-Verlag, 2018.

[18] LiquidRobotics, "Wave glider," https://www.liquid-robotics.com/wave-glider/, 2024, accessed: 2024-08-08.

[19] L. Sciavicco and B. Siciliano, *Modeling and Control of Robot Manipulators*, 2nd ed. London, UK: Springer-Verlag, 2000.

[20] R. E. Sheldahl and P. C. Klimas, "Aerodynamic characteristics of seven symmetrical airfoil sections through 180-degree angle of attack for use in aerodynamic analysis of vertical axis wind turbines," Sandia National Lab.(SNL-NM), Albuquerque, NM (United States), Tech. Rep., 1981.

[21] F. Zhang, J. Thon, C. Thon, and X. Tan, "Miniature underwater glider: Design and experimental results," *IEEE/ASME Transactions on Mechatronics*, vol. 19, no. 1, pp. 394–399, 2013.

[22] NACA, "NACA 0021 airfoil," http://airfoiltools.com/airfoil/details?airfoil=naca0021-il, 2023, accessed: 2023-05-15.

[23] M. Walker and D. Orin, "Efficient dynamic computer simulation of robotic mechanisms," *Journal of Dynamical Systems, Measurement, Control*, vol. 104, no. 3, pp. 205–211, 1982.

[24] R. Featherstone and D. Orin, "Robot dynamics: equations and algorithms," in *Robotics and Automation, 2000. Proceedings. ICRA'00. IEEE International Conference on*, vol. 1. IEEE, 2000, pp. 826–834.

DANIELE DI VITO received the Ph.D. degree in robotics from the University of Cassino and Southern Lazio in March 2020. He is currently a Research Fellow at the University of Cassino and Southern Lazio, where he has co-founded the Spinoff Everybotics SRL, of which he is CEO, and he is with the Interuniversity Research Center on Integrated Systems for the Marine Environment (ISME). In 2018, he spent 4 months as a visiting PhD student at McGill University and Kinova Robotics company, Montreal, Canada. His research interests are about motion planning, kinematic and dynamic control with deep-learning-based collision detection techniques of mobile and base-fixed redundant manipulator systems, both in assistive and underwater robotics. His research activity is focusing on Physics-Informed Neural Networks (PINNs) as well. He has also been involved in several research projects, including the H2020 project ROBUST on seabed mining for the development of the dynamic control layer of an underwater vehicle-manipulator system, and the WAVE project (2022-2023) financed by the Italian Navy on the energy harvesting of ocean waves for vehicle propulsion.

GIUSEPPE GILLINI is a co-founder of EveryBotics S.R.L. and holds a Ph.D. in Methods, Models, and Technologies for Engineering from the University of Cassino and Southern Lazio. His research focuses on assistive and collaborative robotics, human–robot interaction, and fault detection and isolation in multi-robot systems. He has contributed to several international research projects, including collaborations with the German Aerospace Center (DLR) on the integration of brain–computer interfaces with robotic platforms for assistive applications. In addition to his academic work, he has extensive experience in the design and development of web-based systems, with a particular expertise in Angular for building interactive and high-performance applications. His professional activities also include the application of Industry 4.0 technologies to robotics and automation, as well as the development of IoT solutions for monitoring and control. Dr. Gillini is a Certified Ethical Hacker and has delivered talks, corporate training, and technical workshops on robotics, automation, and software engineering. He has authored and co-authored publications in peer-reviewed journals and international conferences in the fields of robotics and human–machine interaction.

This article has been accepted for publication in IEEE Access. This is the author's version which has not been fully edited and content may change prior to final publication. Citation information: DOI 10.1109/ACCESS.2026.3702412

ALESSANDRO COLLEVECCHIO graduated as a technical expert specializing in aircraft construction in July 2000. In September he joined the Navy, attending the Naval Academy in Livorno until 2005, obtaining a master's degree in political science with an international focus. In 2006, he completed specialized training in Antisubmarine Warfare (ASW) at the Naval Academy. Since 2006, he served the Navy as ASW Officer in multiple training and operational activities, in numerous scenarios, tasks and ranks. In 2014 he was appointed Commander of an Italian Navy's ship. In 2017 he left the Navy, becoming a civilian servant in the Ministry of Defense, employed in the field of autonomous vehicles at the Naval Support and Experimentation Centre in La Spezia.

LORENZO BAZZARELLO received the M.Sc. degree in telecommunications engineering, the post-master's degree in underwater electroacoustics and applications, and the Ph.D. degree in underwater electroacoustics and robotics from the University of Pisa, Pisa, Italy, in 2013, 2017, and 2023, respectively. He joined the Italian Navy in 2006 and graduated from the Naval Academy of Livorno, Livorno, Italy, in 2010. From 2013 to 2019, he served with the research branch of the Italian Navy Mine Countermeasure Headquarters. In 2015, he completed specialized training in mine countermeasures at the Naval Academy of Livorno. He is currently an Engineer Officer at the Naval Support and Experimentation Centre of the Italian Navy, La Spezia, Italy. His research interests include high-frequency imaging sonar, acoustic measurement techniques, electroacoustics, underwater robotics, and the application of artificial intelligence to mine countermeasures.

ALBERTO TRAVERSO is Full Professor of Energy Systems at University of Genoa, Italy. He started the academic career as Assistant Professor in 2005 at the Rolls-Royce University Technology Centre in Genoa. Alberto is currently member of the Energy Turbomachinery Network Board since 2024, member of the International Advisory Committee (IAC) for Gas Turbine Society of Japan (GTSJ) since 2013. He has been serving the ASME Turbo Expò Technical Committees and Organizing Committee since more than two decades. He published more than 200 scientific papers, most of them at International conferences and Journals, 22 invited lecturers, 18 patents (Italy, US and World), and received 14 awards. He has been working with several International companies in the field of innovative energy system performance, dynamics and controls.

ANDREA CAFFAZ holds a degree in Electronic Engineering and a Ph.D. in Robotics. He is a founder and senior executive in the field of advanced mechatronics and underwater robotics, with more than 27 years of experience in industrial development and applied research. He is co-founder and long-standing leader of Graal Tech S.r.l., an Italian company specialized in autonomous underwater vehicles, robotic manipulators, and mission-critical mechatronic systems for subsea and defense applications. He has participated in several international research projects and has contributed to the authorship of multiple scientific articles in the fields of robotics and mechatronic systems.

GIANLUCA ANTONELLI is a Full Professor at the ''University of Cassino and Southern Lazio'' and head of the Department of Electrical and Information Engineering. His research interests include marine and industrial robotics, multi-agent systems, identification. He has published more than 60 international journal papers and 130 conference papers, he is the author of the book ''Underwater Robots'' (Springer, 2003, 2006, 2014, 2018) and co-authored the chapter ''Underwater Robotics'' for the Springer Handbook of Robotics (Springer, 2008, 2016). From 2016 to 2021 he has been member elected of the ''IEEE Robotics & Automation Society'' (RAS) Administrative Committee, he has been coordinator of the Eu-Robotics Topic Group in Marine Robotics, he has been secretary of the IEEE-Italy section, he has been chair of the IEEE RAS Italian Chapter, he has been Chair of the IEEE RAS Technical Committee in Marine Robotics. He served on the Editorial Board of the IEEE Transactions on Robotics, IEEE Transactions on Control Systems Technology, Springer Journal of Intelligent Service Robotics. He is an IEEE Fellow since 2021, a Fellow AAIA since 2023, and an AIIA Fellow since 2024. Since October 2020, he was top 1% in the field ''Industrial Engineering & Automation'' according to common metrics and the SCOPUS database (https://data.mendeley.com/datasets/btchxktzyw/4, https://elsevier.digitalcommonsdata.com/datasets/btchxktzyw/3, https://data.mendeley.com/datasets/btchxktzyw/2). Since December 2021, he is in the top 100 Italian scientists according to Google Scholar h-index in the category ''Electronics and Electrical Engineering'' (https://research.com/scientists-rankings/electronics-and-electrical-engineering/it).